Article

# Precise date for the Laacher See eruption synchronizes the Younger Dryas

https://doi.org/10.1038/s41586-021-03608-x

Received: 29 August 2020

Accepted: 4 May 2021

Published online: 30 June 2021

Check for updates

Frederick Reinig[1]✉, Lukas Wacker[2], Olaf Jöris[3,4,5], Clive Oppenheimer[6], Giulia Guidobaldi[7], Daniel Nievergelt[7], Florian Adolphi[8,9], Paolo Cherubini[7,10], Stefan Engels[11], Jan Esper[1,12], Alexander Land[13,14], Christine Lane[6], Hardy Pfanz[15], Sabine Remmele[13], Michael Sigl[16], Adam Sookdeo[2] & Ulf Büntgen[6,7,12,17]

The Laacher See eruption (LSE) in Germany ranks among Europe's largest volcanic events of the Upper Pleistocene[1,2]. Although tephra deposits of the LSE represent an important isochron for the synchronization of proxy archives at the Late Glacial to Early Holocene transition[3], uncertainty in the age of the eruption has prevailed[4]. Here we present dendrochronological and radiocarbon measurements of subfossil trees that were buried by pyroclastic deposits that firmly date the LSE to 13,006 ± 9 calibrated years before present (BP; taken as AD 1950), which is more than a century earlier than previously accepted. The revised age of the LSE necessarily shifts the chronology of European varved lakes[5,6] relative to the Greenland ice core record, thereby dating the onset of the Younger Dryas to 12,807 ± 12 calibrated years BP, which is around 130 years earlier than thought. Our results synchronize the onset of the Younger Dryas across the North Atlantic–European sector, preclude a direct link between the LSE and Greenland Stadial-1 cooling[7], and suggest a large-scale common mechanism of a weakened Atlantic Meridional Overturning Circulation under warming conditions[8–10].

The LSE in central Germany expelled around 20 $km^3$ of tephra[1], making it comparable in magnitude to the 1991 eruption of Mount Pinatubo[11]. Proximal areas were buried by thick pumice fall deposits and ignimbrites[12] (Fig. 1), and Laacher See tephra (LST) fallout from ash clouds reached Northern Italy and Saint Petersburg (Extended Data Fig. 1), yielding a distinctive marker bed that can be recognized in terrestrial and lacustrine records[3]. The generally accepted age of the eruption of 12,880 ± 40 $BP_{MFM}$ derives from the Meerfelder Maar varve (MFM) record[5]. Further estimates are associated with much higher uncertainties and define a time window[4] for the eruption of around 13,200–12,840 BP. The only independent age estimate was obtained from radiometric ($^{40}Ar/^{39}Ar$) dating of the Upper LST deposits (12,900 ± 560 BP)[13], but it suffers from considerable uncertainty. Owing to its widespread dispersal, the LST represents a decisive Late Glacial isochron, enabling synchronization of proxy archives over a wide area[3]. Although evidence of the regional environmental impacts of the eruption is well-documented[2], its influence on the climate of the Northern Hemisphere is ambiguous, owing in part to poor constraints of its sulfur yield to the atmosphere (estimates range between 7 and 300 teragrams of sulfur dioxide[2,14]).

What is clear is that the eruption took place during the later phase of the Allerød (AL) interstadial, and around 200 varve-counted years before the onset of the Younger Dryas (YD) cold interval[12]. Despite decades of intensive research, the lingering dating uncertainty for the LSE has limited the development of an absolutely dated European Late Glacial proxy chronology, intercomparison of European terrestrial and Arctic glaciochemical records, and evaluation of the North Atlantic climate transition from the Late Glacial to the Early Holocene, including the speculated role of the LSE in triggering Greenland Stadial 1 (GS-1)[7]. However, the development of a high temporal resolution radiocarbon ($^{14}C$) calibration curve based on Late Glacial subfossil trees from Switzerland[15] paved the way for progress in dating the LSE, leading us to conduct new dendrochronological and $^{14}C$ dating studies of subfossil trees that were killed during the eruption and engulfed in its deposits. This approach provides an independent and absolute calibration of various Late Glacial proxy archives.

## Multi-parameter dating

We examined three birch (*Betula* sp.) and two poplar (*Populus* sp.) trunks found in LSE deposits near the crater (see Methods, Fig. 1 and Extended Data Fig. 2). Poplar 1 is the only non-carbonized sample, and is therefore suitable for macroscopic tree-ring width measurements (see Methods). Wood anatomical thin sectioning[16] and X-ray

[1]Department of Geography, Johannes Gutenberg University, Mainz, Germany. [2]Laboratory of Ion Beam Physics, ETH Zurich, Zurich, Switzerland. [3]Römisch-Germanisches Zentralmuseum–MONREPOS Archaeological Research Centre and Museum for Human Behavioural Evolution, Neuwied, Germany. [4]Institute of Ancient Studies, Department of Prehistoric and Protohistoric Archaeology, Johannes Gutenberg University, Mainz, Germany. [5]Key Laboratory of Western China's Environmental Systems (Ministry of Education), College of Earth and Environmental Sciences, Lanzhou University, Lanzhou, China. [6]Department of Geography, University of Cambridge, Cambridge, UK. [7]Swiss Federal Research Institute WSL, Birmensdorf, Switzerland. [8]Alfred Wegener Institute, Helmholtz Center for Polar and Marine Research, Bremerhaven, Germany. [9]Department of Geosciences, University of Bremen, Bremen, Germany. [10]Department of Forest and Conservation Sciences, University of British Columbia, Vancouver, British Columbia, Canada. [11]Department of Geography, Birkbeck University of London, London, UK. [12]Global Change Research Institute of the Czech Academy of Sciences (CzechGlobe), Brno, Czech Republic. [13]Institute of Biology (190a), University of Hohenheim, Stuttgart, Germany. [14]Silviculture & Forest Growth and Yield, University of Applied Forest Sciences, Rottenburg am Neckar, Germany. [15]Institute of Applied Botanics and Volcanic Biology, Universität Duisburg-Essen, Essen, Germany. [16]Climate and Environmental Physics, Physics Institute, Oeschger Centre for Climate Change Research, University of Bern, Bern, Switzerland. [17]Department of Geography, Faculty of Science, Masaryk University, Brno, Czech Republic. ✉e-mail: reinig@geo.uni-mainz.de

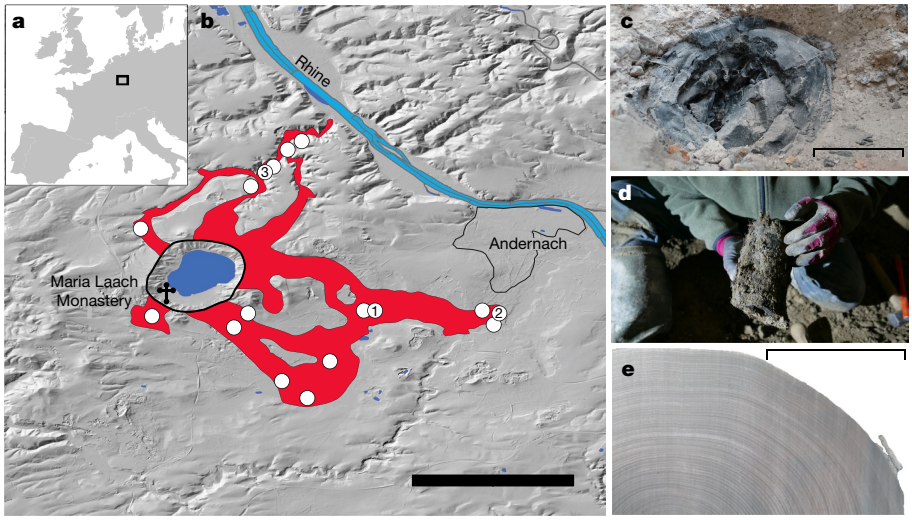


**Fig. 1 | LSE wood finds. a**, **b**, Location of the Laacher See (**a**) and the discovered subfossil wood samples (white circles) within the Middle Laacher See tephra (MLST) ignimbrite deposits (red shading) near Andernach, Germany (**b**). Maps are modified from a previously published study[12]. **c**, **d**, Subfossil trees buried in a tuff quarry near Meurin (circle 1) (**c**) and near Miesenheim excavated in 2019 (circle 2) (**d**). **e**, X-ray densitometry image of a charcoal sample of Birch 1 (circle 3). The map is produced using QGIS. Scale bars, 5 km (**b**), 10 cm (**c**) and 5 cm (**e**).

densitometry[17] of the charcoal samples enabled the precise identification of ring boundaries (supplementary table 1 hosted at https://www.ncdc.noaa.gov/paleo/study/33194) and dendrochronological cross-dating. Determination of the LSE age was supported by the presence of the outermost ring and bark. Birch 1 and Poplar 1 contained 104 and 95 tree rings, respectively (Fig. 2 and Extended Data Table 1). The presence of initial early wood cells before the bark on Poplar 1 corroborates previously reported sedimentological, palaeobotanical and trace fossil evidence for a spring to early summer eruption[12].

We performed 157 high-resolution $^{14}$C measurements (see Methods) for Birch 1, Poplar 1 and Poplar 2 (Extended Data Table 1 and supplementary tables 2–4 hosted at https://www.ncdc.noaa.gov/paleo/study/33194). Wiggle-matching of the new $^{14}$C values from our 104-year-long pre-LSE tree-ring chronology against the Swiss Late Glacial Master Radiocarbon (SWILM-$^{14}$C) dataset[15,18] (Methods, Extended Data Fig. 3 and supplementary table 8 hosted at https://www.ncdc.noaa.gov/paleo/study/33194) dates the LSE to 13,006 ± 9 calibrated (cal.) BP ($2\sigma$) (Fig. 3a). Agreement of high- and low-frequency $\Delta^{14}$C changes from 13,111–13,007 cal. BP between the highly resolved isotopic measurements from the pre-LSE sequence and SWILM-$^{14}$C reference constrains the uncertainty. Note in Fig. 3a that the rapid increase in $^{14}$C between 13,110 and 13,090 cal. BP positions the pre-LSE sequence precisely and does not allow for ambiguity. The $^{14}$C excursion centred at 13,055 cal. BP not only validates the dating between the birch and poplar data, but also supports synchronization relative to the SWILM-$^{14}$C record.

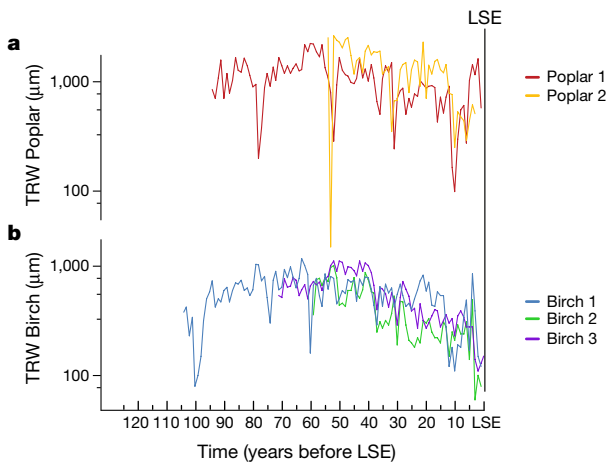


**Fig. 2 | Dendrochronological cross-dating of pre-LSE tree-ring width measurements. a**, **b**, Two poplar (**a**) and three birch (**b**) samples, aligned along the bark layer of Poplar 1 and Birch 3. All of the trees had been killed and buried during the LSE, and were excavated from tephra deposits. Note the logarithmic scales. TRW, tree-ring width.

## North Atlantic–European archives

Our LSE age, which is around 130 years older than previously reported, contributes to an independent, near-absolute tephrostratigraphic tie-point for the Late Glacial, and sheds light on the controversial debate of the timing, pace, duration and spatiotemporal transgression of North Atlantic climate changes. The transition from the Late Glacial to Early Holocene is characterized by strong climatic and environmental fluctuations, including the approximately 1,100-year-long YD, the last severe cold reversal before the Holocene[19–23]. The onset of the YD is recognized as time-transgressive in European proxy archives, indicating that regional and delayed responses to climatic changes occurred that are recorded earlier in Greenland ice cores[24–26]. Acknowledging different sampling resolutions and dating uncertainties of the various archives, the offset between Greenland GS-1 and the European YD has been estimated to be up to two centuries[6,27].

Our LSE age of 13,006 ± 9 cal. BP shifts many European proxy records to older ages and challenges the previously hypothesized delayed and stepwise southward migration of the YD[6] (Extended Data Fig. 4a). The varved lake sediments from MFM, which is around 50 km southwest of Laacher See, represent the most reliable master chronology for the YD in central Europe[5]. This record[5] places the LSE at 12,880 ± 40 $BP_{MFM}$. However, the MFM chronology depends on the Ulmener Maar Tephra dated at 11,000 varve years BP and single $^{14}$C dates[28], challenging its derived LSE date. Our LSE age shifts the MFM record by 126 years towards older ages during the late AL. As around 200 varve years have been recorded consistently in annually resolved European varved records between the LSE fallout horizon and the beginning of the YD[19,29–31], the onset of the YD is necessarily revised to 12,807 ± 12 cal. BP ($2\sigma$) (Methods and Extended Data Table 2).

The beginning of GS-1 cooling is dated to 12,846 (±138 years) $BP_{GICC05}$ (ref. [32]) on the Greenland Ice Core Chronology 2005 timescale (GICC05)[23] (Extended Data Fig. 4a). Our revised older age for the onset

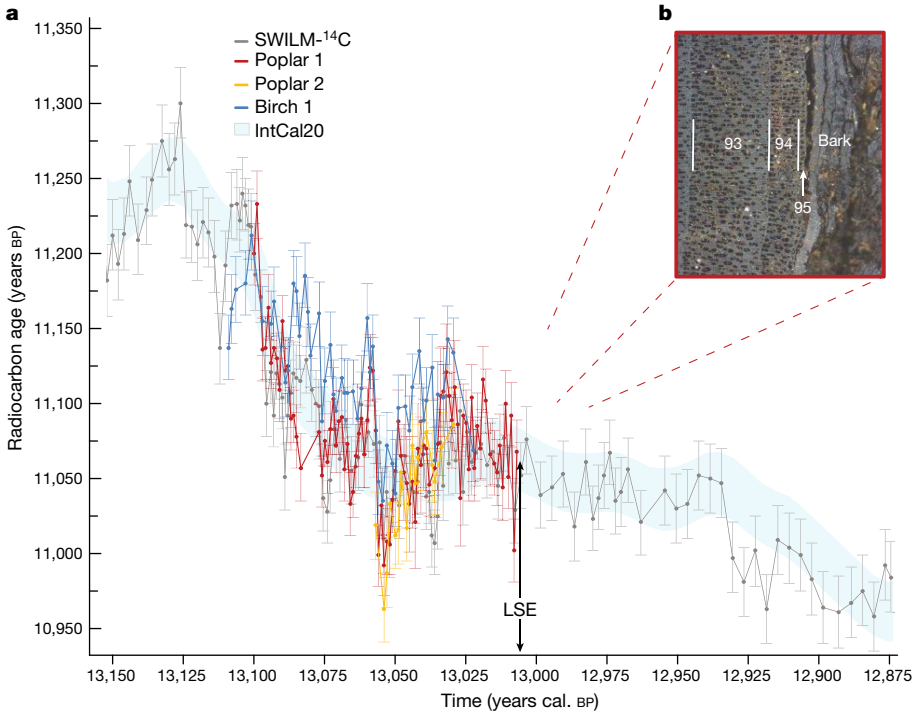


**Fig. 3 | Dating of the LSE. a**, High-resolution $^{14}$C measurements from three tree-ring sequences recovered from LST deposits and wiggle-matched to the Swiss Late Glacial reference (SWILM-$^{14}$C) on the $^{14}$C timescale[15,18]. Blue shading denotes IntCal20 reference[18]. Data are shown with 1$\sigma$ errors. **b**, Tree-ring boundaries and bark identified macroscopically on Poplar 1.

of the YD recorded in the European lakes now aligns with the Greenland Interstadial 1a–Greenland Stadial 1 (GI-1a–GS-1) transition (Fig. 4b–d), and therefore synchronizes the onset of GS-1 and the YD. On the basis of the synchronization of tree-ring $^{14}$C and ice-core beryllium-10 ($^{10}$Be) data, both timescales are consistent within about −12/+21 years (2$\sigma$) around this period in time[33]. This synchronization thereby bypasses the cumulative counting error of the ice-core timescale for the GS-1 versus YD comparison. Stable oxygen isotope ($\delta^{18}$O) measurements of sediment cores from the European Alpine lakes Ammersee[34] and Mondsee[35], both of which contain LST, are based on age models that incorporate the LSE age from the MFM. Revising these models with our LSE age shows that the isotopic AL/YD transition is synchronous with the climate transition in Greenland (Fig. 4c, d). Identification of LSE tephra in Greenland ice cores would yield the first near-absolute time marker of the pre-Holocene GICC05 chronology. Correcting for differences between tree-ring and ice-core timescales within this period[33], our LSE age now confines the search window in ice cores to a range between 13,015 and 12,975 $BP_{GICC05}$ (Methods, Extended Data Fig. 5 and Extended Data Table 3).

## Atlantic–European climate mechanisms

Our study demonstrates that the Greenland GI-1–GS-1 transition coincided with the European AL/YD cooling. The temporal match between Greenland ice core and central European climate proxies suggests that the last major Northern Hemisphere cooling interval before the Holocene was initiated and steered by an abrupt climate system change that instantly affected the whole North Atlantic region. This finding is in line with a revised calibration of $^{14}$C data from Kråkenes Lake in western Norway[26,36] (Fig. 4b) using the 2020 International Radiocarbon Calibration Curve (IntCal20)[18]. The improved calibration (Extended Data Table 4) shows that the AL/YD boundary in Scandinavia coincides with the proposed AL/YD transition in lacustrine varve records from Central Europe (Methods). Our results further rule out any direct impact of the LSE on the transition into GS-1, as suggested previously[7], since the revised eruption date substantially precedes the cooling identified in Greenland ice core records[32].

The trigger of the GS-1 cold reversal has been attributed to a sudden meltwater release from the Laurentide Ice Sheet in North America that weakened the Atlantic Meridional Overturning Circulation (AMOC)[8]. Understanding the exact timing of such a large-scale climate transition is important in the context of recent global warming, which is also characterized by a weakened AMOC[9]. The GS-1–YD cold reversal, therefore, represents a natural analogue to the predicted consequences of a weakened AMOC under global warming[9,10]. The improved proxy synchronization that arises from our $^{14}$C-tuned dating of the LSE promises improved insights into the triggers and extent of the YD[8,37,38], which may—in turn—inform understanding of the conditions that are conducive to any future AMOC shutdown.

## Online content

Any methods, additional references, Nature Research reporting summaries, source data, extended data, supplementary information, acknowledgements, peer review information; details of author contributions and competing interests; and statements of data and code availability are available at https://doi.org/10.1038/s41586-021-03608-x.


1. Schmincke, H.-U. in *Mantle Plumes* (eds Ritter, J. R. R. & Christensen, U. R.) 241–322 (Springer, 2007).
2. Schmincke, H.-U., Park, C. & Harms, E. Evolution and environmental impacts of the eruption of Laacher See Volcano (Germany) 12,900 a BP. *Quat. Int.* **61**, 61–72 (1999).
3. Lane, C. S., Blockley, S. P. E., Bronk Ramsey, C. & Lotter, A. F. Tephrochronology and absolute centennial scale synchronisation of European and Greenland records for the last glacial to interglacial transition: a case study of Soppensee and NGRIP. *Quat. Int.* **246**, 145–156 (2011).
4. Reinig, F. et al. Towards a dendrochronologically refined date of the Laacher See eruption around 13,000 years ago. *Quat. Sci. Rev.* **229**, 106128 (2020).
5. Brauer, A., Endres, C. & Negendank, J. F. W. Lateglacial calendar year chronology based on annually laminated sediments from Lake Meerfelder Maar, Germany. *Quat. Int.* **61**, 17–25 (1999).
6. Rach, O., Brauer, A., Wilkes, H. & Sachse, D. Delayed hydrological response to Greenland cooling at the onset of the Younger Dryas in western Europe. *Nat. Geosci.* **7**, 109–112 (2014).
7. Baldini, J. U. L., Brown, R. J. & Mawdsley, N. Evaluating the link between the sulfur-rich Laacher See volcanic eruption and the Younger Dryas climate anomaly. *Clim. Past* **14**, 969–990 (2018).
8. Broecker, W. S., Peteet, D. M. & Rind, D. Does the ocean–atmosphere system have more than one stable mode of operation? *Nature* **315**, 21–26 (1985).
9. Rahmstorf, S. et al. Exceptional twentieth-century slowdown in Atlantic Ocean overturning circulation. *Nat. Clim. Change* **5**, 475–480 (2015).
10. Caesar, L., Rahmstorf, S., Robinson, A., Feulner, G. & Saba, V. Observed fingerprint of a weakening Atlantic Ocean overturning circulation. *Nature* **556**, 191–196 (2018).
11. Holasek, R. E., Self, S. & Woods, A. W. Satellite observations and interpretation of the 1991 Mount Pinatubo eruption plumes. *J. Geophys. Res.* **101**, 27635–27655 (1996).

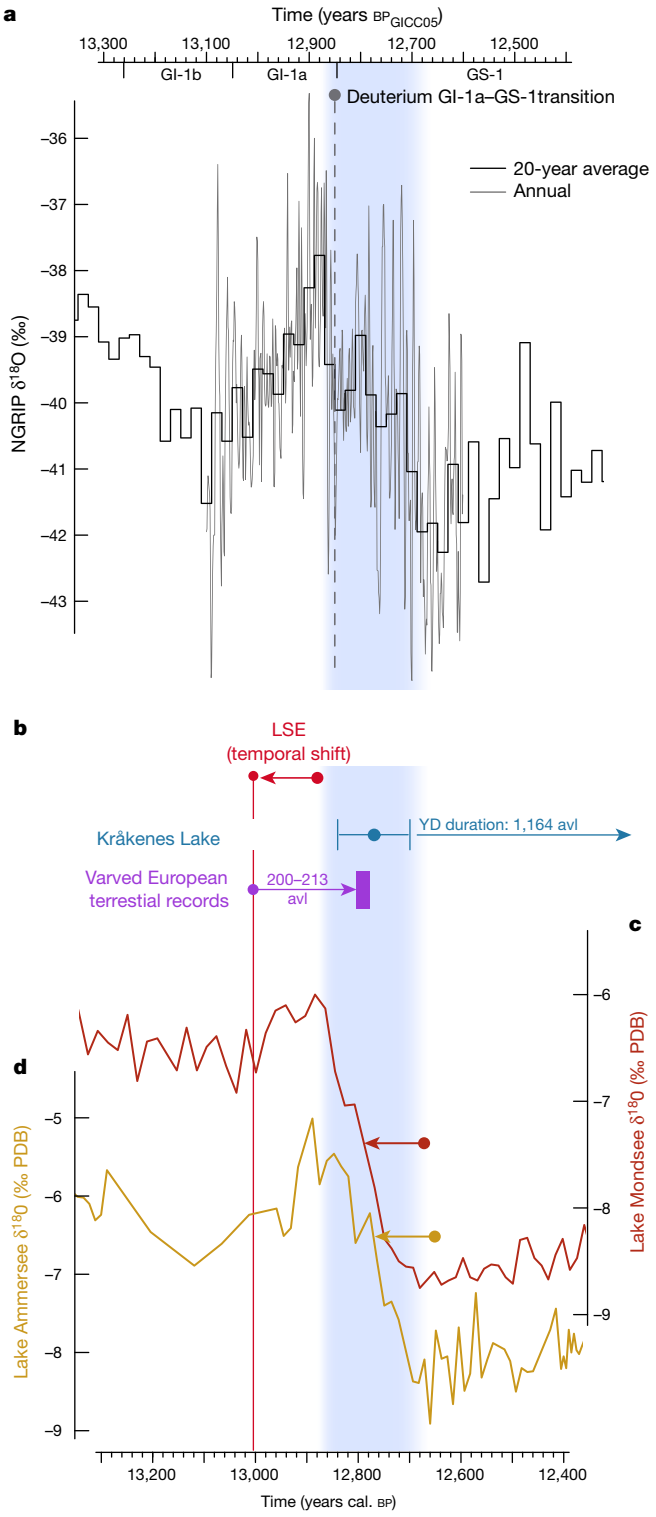


**Fig. 4 | Multi-proxy alignment of circum-Atlantic records. a**, North Greenland Ice Core Project (NGRIP) oxygen isotopes ($\delta^{18}O$; relative to the Vienna Standard Mean Ocean Water standard) in 20-year (black)[23] and annual (grey)[31] resolution on the GICC05 timescale[23]. Light blue shading denotes the GI-1a–GS-1 transition in $\delta^{18}O$ and the vertical grey dashed line marks the transition in deuterium excess[32]. **b**, Temporal shift of the mean MFM LST age estimate (12,880 varve years BP$_{MFM}$)[28] by 126 years towards older ages. Mean ±1$\sigma$ AL/YD boundary ages obtained from Kråkenes Lake (Norway,)[27] calibrated against IntCal20[18], and mean and standard deviation (purple bar) of European varved terrestrial records (Soppensee, Switzerland[39]; Rehwiese, Germany[29]; Trzechowskie, Poland[40]) aligned relative to our newly established LSE age estimate (red vertical line), which consistently indicated approximately 200–213 annual varves (avl) between the LST and the AL/YD boundary, suggesting a YD onset at around 12,807 cal. BP. **c**, **d**, Realigned LST-containing Late Glacial alpine $\delta^{18}O$ records from Mondsee[35] and Lake Ammersee[34] (relative to Vienna PeeDee Belemnite (PDB) standard). Arrows indicate the temporal shift of 126 years towards older ages. Data in **a** are plotted according to the GICC05 timescale with respect to AD 1950; data in **b**–**d** are plotted on the calibrated $^{14}C$ timescale (cal. BP (AD 1950)).


12. Baales, M. et al. Impact of the Late Glacial eruption of the Laacher See volcano, central Rhineland, Germany. *Quat. Res.* **58**, 273–288 (2002).
13. van den Bogaard, P. $^{40}Ar/^{39}Ar$ ages of sanidine phenocrysts from Laacher See tephra (12,900 yr BP): chronostratigraphic and petrological significance. *Earth Planet. Sci. Lett.* **133**, 163–174 (1995).
14. Textor, C., Sachs, P. M., Graf, H.-F. & Hansteen, T. H. The 12 900 years BP Laacher See eruption: estimation of volatile yields and simulation of their fate in the plume. *Geol. Soc. Lon. Spec. Pub.* **213**, 307–328 (2003).
15. Reinig, F. et al. New tree-ring evidence for the Late Glacial period from the northern pre-Alps in eastern Switzerland. *Quat. Sci. Rev.* **186**, 215–224 (2018).
16. Reinig, F. et al. Introducing anatomical techniques to subfossil wood. *Dendrochronologia* **52**, 146–151 (2018).
17. Schweingruber, F. H. *Tree Rings: Basics and Applications of Dendrochronology* (Kluwer Academic Publishers, 1988).
18. Reimer, P. J. et al. The IntCal20 Northern Hemisphere radiocarbon age calibration curve (0–55 cal kBP). *Radiocarbon* **62** 725–757 (2020).
19. Brauer, A., Haug, G. H., Dulski, P., Sigman, D. M. & Negendank, J. F. W. An abrupt wind shift in western Europe at the onset of the Younger Dryas cold period. *Nat. Geosci.* **1**, 520–523 (2008).
20. Haflidason, H., Sejrup, H. P., Klitgaard Kristensen, D. & Johnsen, S. Coupled response of the late glacial climatic shifts of northwest Europe reflected in Greenland ice cores: evidence from the northern North Sea. *Geology* **23**, 1059–1062 (1995).
21. Hughen, K. A., Southon, J. R., Lehman, S. J. & Overpeck, J. T. Synchronous radiocarbon and climate shifts during the last deglaciation. *Science* **290**, 1951–1955 (2000).
22. Johnsen, S. J. et al. Irregular glacial interstadials recorded in a new Greenland ice core. *Nature* **359**, 311–313 (1992).
23. Rasmussen, S. O. et al. A stratigraphic framework for abrupt climatic changes during the Last Glacial period based on three synchronized Greenland ice-core records: refining and extending the INTIMATE event stratigraphy. *Quat. Sci. Rev.* **106**, 14–28 (2014).
24. Lane, C. S., Brauer, A., Blockley, S. P. E. & Dulski, P. Volcanic ash reveals time-transgressive abrupt climate change during the Younger Dryas. *Geology* **41**, 1251–1254 (2013).
25. Muschitiello, F. et al. Fennoscandian freshwater control on Greenland hydroclimate shifts at the onset of the Younger Dryas. *Nat. Commun.* **6**, 8939 (2015).
26. Obreht, I. et al. An annually resolved record of Western European vegetation response to Younger Dryas cooling. *Quat. Sci. Rev.* **231**, 106198 (2020).
27. Lohne, Ø. S., Mangerud, J. & Birks, H. H. Precise $^{14}C$ ages of the Vedde and Saksunarvatn ashes and the Younger Dryas boundaries from western Norway and their comparison with the Greenland Ice Core (GICC05) chronology. *J. Quat. Sci.* **28**, 490–500 (2013).
28. Brauer, A. et al. High resolution sediment and vegetation responses to Younger Dryas climate change in varved lake sediments from Meerfelder Maar, Germany. *Quat. Sci. Rev.* **18**, 321–329 (1999).
29. Neugebauer, I. et al. A Younger Dryas varve chronology from the Rehwiese palaeolake record in NE-Germany. *Quat. Sci. Rev.* **36**, 91–102 (2012).
30. Lotter, A. F., Eicher, U., Siegenthaler, U. & Birks, H. J. B. Late-glacial climatic oscillations as recorded in Swiss lake sediments. *J. Quat. Sci.* **7**, 187–204 (1992).
31. Merkt, J. & Müller, H. Varve chronology and palynology of the Lateglacial in Northwest Germany from lacustrine sediments of Hämelsee in Lower Saxony. *Quat. Int.* **61**, 41–59 (1999).
32. Steffensen, J. P. et al. High-resolution Greenland ice core data show abrupt climate change happens in few years. *Science* **321**, 680–684 (2008).
33. Adolphi, F. et al. Connecting the Greenland ice-core and U/Th timescales via cosmogenic radionuclides: testing the synchroneity of Dansgaard–Oeschger events. *Clim. Past* **14**, 1755–1781 (2018).
34. von Grafenstein, U., Erlenkeuser, H., Brauer, A., Jouzel, J., & Johnsen, S. J. A mid-European decadal isotope-climate record from 15,500 to 5000 years B.P. *Science* **284**, 1654–1657 (1999).
35. Lauterbach, S. et al. Environmental responses to Lateglacial climatic fluctuations recorded in the sediments of pre-Alpine Lake Mondsee (northeastern Alps). *J. Quat. Sci.* **26**, 253–267 (2011).
36. Lohne, Ø. S., Mangerud, J. & Birks, H. H. IntCal13 calibrated ages of the Vedde and Saksunarvatn ashes and the Younger Dryas boundaries from Kråkenes, western Norway. *J. Quat. Sci.* **29**, 506–507 (2014).
37. Condron, A. & Winsor, P. Meltwater routing and the Younger Dryas. *Proc. Natl Acad. Sci. USA* **109**, 19928–19933 (2012).
38. Renssen, H. et al. Multiple causes of the Younger Dryas cold period. *Nat. Geosci.* **8**, 946–949 (2015).
39. Hajdas, I. et al. AMS radiocarbon dating and varve chronology of Lake Soppensee: 6000 to 12000 $^{14}C$ years BP. *Clim. Dyn.* **9**, 107–116 (1993).
40. Wulf, S. et al. Tracing the Laacher See tephra in the varved sediment record of the Trzechowskie palaeolake in central Northern Poland. *Quat. Sci. Rev.* **76**, 129–139 (2013).

# Methods

### Sample provenance and description

An area of more than 1,000 km$^3$ was buried below the LST[11]. Within an approximately 10 km radius around the Laacher See, where LST fallout deposits and ignimbrites reached considerable thicknesses, and of the lower Neuwied Basin, where temporarily lakes had syneruptively formed[41], finds of diaspores, plant macrofossils[12] and leaf imprints[42] document a species-rich interstadial Late Glacial hemiboreal vegetation. Over the past 200 years, botanical macro-remains have been randomly gathered, often by private collectors[42]. Since the 1950s, material was sampled during geoscientific fieldwork and samples were submitted for radiocarbon dating[43,44]. Over the past 40 years, some tree macro-fossils were collected by different science institutes, including the Universities of Cologne, Hohenheim and Duisburg-Essen. The most systematic collection is stored in the MONREPOS Archaeological Research Centre and Museum for Human Behavioural Evolution near Neuwied (Germany), a competence centre of the Römisch-Germanisches Zentralmuseum (RGZM), where material unearthed during extensive geoarchaeological work in and around the Neuwied Basin has been archived since the 1980s[12,45,46] (Extended Data Fig. 2). During a recent field campaign in January 2019 well-preserved trees buried within LST ignimbrites (ignimbrites and co-ignimbrites of the MLST deposits) were documented at a new locality near Miesenheim.

Within the more loosely packed pumice fallout deposits, moulds of trees still standing upright have been observed frequently[41], whereas in situ subfossil and/or charred trees were only preserved within the compact ignimbritic MLST deposits[47]. These filled the pre-LSE near-vent valleys and depressions by approximately 10–20-m thick deposits to the south and southeast of the Laacher See (Nette Valley ignimbrites) and up to 60 m to the north and northeast (Brohl Valley ignimbrites) during the middle phase of the LSE (Fig. 1 and Extended Data Fig. 2). At some localities such as in Brohl (sites 1 and 2)[45] and in Kruft[47], smaller stands of trees were documented during roadwork and quarrying, respectively, and excavated using archaeological methods. At the site of Miesenheim 2 (ref. [12]), an entire forest floor with poplar tree stems and roots was excavated and documented over an area of several hundred square metres in the mid-1980s[46]. At this site, however, the preserved wood was strongly mouldered, which made it impossible to preserve. Other tree macro-fossils found at various sites within the region include trees tilted by syneruptive blasts (and/or numerous charred wood fragments), as were first discovered at Thür[48]. Further such discoveries have been documented at Tönisstein and other Brohl Valley exposures, in the Meurin quarries near Kruft, in Miesenheim 4 and at the 2019 Miesenheim locality, where we were able to excavate and document a series of well-preserved tilted trees with diameters up to 20 cm, buried within MLST ignimbrites.

For the present study, five tree samples (two poplar and three birch trees) with the most intact wood quality and structure were chosen for tree-ring width (TRW) analysis (supplementary table 1 hosted at https://www.ncdc.noaa.gov/paleo/study/33194). The samples, for which more detailed information is available, consistently derive from trees that have been preserved and discovered within MLST deposits that buried the trees at their immediate growth sites. In Miesenheim 2, Kruft and in the Brohl Valley, trees were documented standing upright, embedded within basal MLST ignimbrites. With the succeeding ignimbrite flow through the valley, the trunks were capped at approximately 4 m length. The observed upright position and the occasional presence of bark on the tree samples indicate that the trees were still alive before their burial. Two subfossil tree finds made by monks and provided by the University of Duisburg-Essen were most likely excavated during renovation works in the immediate vicinity around the monastery and must have been directly located within the LSE ignimbrites and/or the denser-packed co-ignimbritic (namely, 'Britz') layers within the pumice fallout deposits (both types of deposits are assigned to the MLST), given their excellent preservation. The same must be assumed for a sample retrieved from an excursion and made available by the University of Hohenheim. Intrusion of material can be excluded, given the thickness of LST deposits, the late AL $^{14}$C dates and the preservation status of the samples studied. Conservation within the dense ignimbrites enabled the recovery of the bark on two samples (Extended Data Table 1), still attached to the outer sapwood. With the exception of Poplar 1, which had still intact wood cellulose, the preserved tree samples have been carbonized within the compact ignimbrites.

### TRW measurement and cross-dating

At the Swiss Federal Research Institute for Forest, Snow and Landscape WSL in Birmensdorf (Switzerland) wood anatomical transverse (cross) sections were taken, classifying the charcoal samples either as birch (*Betula* sp.) or poplar (*Populus* sp.). Exact tree-ring boundaries are often difficult to identify in broadleaved species and classic microscopic measurements were hindered through narrow rings and the carbonized status of the samples. Ensuring accurate tree-ring boundary identification, wood anatomical thin sectioning[16] as well as X-ray densitometry[17] were applied. Thin sections provided insight into the outer tree-ring identification, whereas X-ray images of carefully cut 0.2–0.5-cm-thick discs enabled multi-radius measurements across the samples. At least four TRW radii were measured from each charcoal sample using a LINTAB measuring device with a precision of 0.01 mm in combination with TSAPWin software[49]. X-ray films were measured on a Walesch 2003 X-ray densitometer using WalDendro V1.10 software, which also had a precision of 0.01 mm. Visual cross-dating was performed within TSAPWin software[49]. Macroscopic TRW measurements of Poplar 1 were performed at the University of Hohenheim with an identical measurement set-up as at the WSL.

### Radiocarbon sample preparation and measurement

On the basis of the cross-dated TRW sequences, 0.8–1.0-cm-wide wood tracks were cut from three tree samples (Poplar 1, Poplar 2 and Birch 1), including the pith and outer most rings of each tree. Rings were manually cut with a scalpel, if possible, in annual or bi-annual resolution providing at least 20 mg of organic material. Special care was taken to prevent any contamination, particularly from neighbouring tree rings. High-resolution radiocarbon ($^{14}$C) Accelerator Mass Spectrometer (AMS) measurements[50–52] were performed at the Laboratory of Ion Beam Physics at ETH Zurich (Switzerland) on the 'Mini Radiocarbon Dating System' (MICADAS). The base–acid–base–acid–bleach method[53] was cautiously applied to extract holocellulose from the intact wood samples. The same treatment was applied to the delicate charcoal samples to isolate the most stable compounds from any external contamination for radiocarbon dating. All samples were, thereafter, graphitized with an AGE system[53]. The ETH quality protocol[54] was applied to ensure the accuracy and comparability of the $^{14}$C results through continuous monitoring of $^{14}$C blanks, standards and reference material.

### Swiss radiocarbon reference dataset

The collection of subfossil Late Glacial wood from Switzerland[15] and corresponding atmospheric $^{14}$C level changes dataset[18], SWILM-$^{14}$C, provides a well-dated (±8 years; 2$\sigma$) and temporally highly resolved reference for precise $^{14}$C matching. In comparison to the recently released International Calibration Curve 2020 (IntCal20)[18], the SWILM-$^{14}$C record—which is derived from a single long-lived tree from this period, GAEN0071 (supplementary table 5 hosted at https://www.ncdc.noaa.gov/paleo/study/33194)—represents a record with higher temporal resolution. Additionally, 118 $^{14}$C measurements from two trees (supplementary tables 6, 7 hosted at https://www.ncdc.noaa.gov/paleo/study/33194), which originated from the Swiss tree-ring chronology Daettnau 3 (ref. [55]), enabled us to match the pre-LSE tree-ring $^{14}$C data to an extended reference, termed SWILM-$^{14}C_{plus}$. It is important to note that the dendrochronological placement of Daettnau 3 in the SWILM-$^{14}$C

record is tentative. We therefore consider the matching results to the SWILM-$^{14}C_{plus}$ record only as an additional test to the results obtained from the SWILM-$^{14}C$ data.

### Radiocarbon wiggle-matching with OxCal

For the $^{14}C$ calibration, 85 $^{14}C$ measurements from Poplar 1 were wiggle-matched against both the SWILM-$^{14}C$ and the extended SWILM-$^{14}C_{plus}$ records using the D_Sequence function in OxCal 4.3[56,57] (see dating results for Poplar 2 and Birch 1 below). The calibration curve was built applying a Savitzky–Golay filter (order, 2; frame length, 11) and the possible offset was set to ±50 years. The wiggle-matching analysis indicates overall good agreement of all Poplar 1 $^{14}C$ dates to the SWILM-$^{14}C$ reference, dating the outermost ring of the sample to 13,007 cal. BP (±1 year; 2$\sigma$). Calibration of Poplar 1 with SWILM-$^{14}C_{plus}$ indicates 13,006 cal. BP (±1 year; 2$\sigma$) as the date of the final ring. Taking into account the underlying reference uncertainty of ±8 years of the SWILM-$^{14}C$ record, we obtain an absolute uncertainty of ±9 years for both wiggle-matches. OxCal results for Birch 1 and Poplar 2 support this wiggle-match (Extended Data Fig. 6).

### Radiocarbon wiggle-matching with a least-square fit

In addition to wiggle-matching results from OxCal, $^{14}C$ sampled trees from the pre-LSE tree-ring chronology were matched to SWILM-$^{14}C$ and SWILM-$^{14}C_{plus}$, such that the $\chi^2$ ($\chi(x)^2$) becomes minimal for an assumed age $x$ for the outermost tree ring (waney edge) before the eruption[52]:

$$\chi(x)^2 = \sum_{i=1}^{n} \frac{(R_i - \bar{C}_{(x-r_i)} - \text{offset})^2}{(\delta R_i^2 + \delta \bar{C}_{(x-r_i)})^2}$$

where $R_i \pm \delta R_i$ are the measured values for the measured $^{14}C$ concentrations of the sample and $\bar{C}_{(x-r_i)} \pm \delta \bar{C}_{(x-r_i)}$ represents the $^{14}C$ concentrations of the SWILM-$^{14}C$ curve for the year $(x - r_i)$, where $r_i$ is the tree-ring number starting with ring number 0 as the final ring of the tree. The values of $\chi(x)^2$ for the most likely matches are given in Extended Data Fig. 3. When tree rings were sampled at a lower temporal resolution, $^{14}C$ values of the trees with higher resolution were combined to match the lower resolution for the $\chi^2$ test. The offset was individually adjusted to find the overall best fit.

### Radiocarbon dating uncertainty

The application of the Oxcal D_Sequence function and the least $\chi^2$ test yielded similar results, indicating an LSE age of 13,006 cal. BP (±9 years; 2$\sigma$). We consider our result to be robust, as testing various combinations between samples and references produced age estimates within the derived age error. Although the $^{14}C$ measurements from Poplar 1, which originated from whole wood, indicated most consistent dating results, $^{14}C$ measurements from the carbonized wood of Birch 1 indicates a systematic offset. Nevertheless, the measurements follow the overall $^{14}C$ structure and outline similar LSE age estimates. We speculate that the observed systematic offset of the charcoal sample is either a result of the direct carbonization process within the hot LSE sediments, later contamination during preservation[58], or related to the injection of magmatic carbon dioxide into the samples during its lifetime, for example through regional groundwater affected by volcanic processes[59]. Dating results from carbonized Poplar 2 are consistent with Poplar 1. We deduce that the only offset between the samples in the period between 13,090 cal. BP and 13,075 cal. BP is caused by the poor wood quality of the Poplar 1 tree rings, for which only selected years could be sampled and $^{14}C$ measurements performed. Precise $^{14}C$ placements were only feasible through the unique high resolution of performed $^{14}C$ measurements and subsequent insight into the $^{14}C$ fine structure. Additionally, the now obtained number of tree rings more than 100 years before the eruption is crucial to exceed the $^{14}C$ plateau, a critical aspect that previous $^{14}C$ dating attempts of charcoal remnants found within the LSE deposits did not achieve[60].

### YD onset estimation

The revised date of the LSE now enables us to more precisely estimate the onset of the YD to approximately 12,807 cal. BP (±12 years; 2$\sigma$), based on the standard deviation of the available counting uncertainties of annually laminated lake sediment records containing LSE evidence as well as high-resolution palaeobotanical evidence indicating the onset of the YD (Extended Data Table 2). We recognize that our result is, however, limited by the systematic error based on the individual record and sampling strategy defining the onset of the YD. The shift in sedimentation in the MFM record indicates a sharp transition into the YD[5]. Defining the onset of the YD in pollen records is subject to (1) where the pollen samples are placed, (2) what the pollen sampling resolution is, and (3) how fast vegetation actually responded to climate deterioration. A lag in the pollen signal relative to the climatic shift can be expected, as the ecosystem response presumably occurred with a delay[61]. For example, pollen-percentage diagrams from the MFM outline a slower transition compared to pollen-accumulation rates, reflecting a more immediate response to the onset of the YD[62]. The chronological accuracy of AL/YD palaeo-records is now reaching a point where it is actually more precise than the sampling resolution of the underlying proxy information, challenging previous sampling strategies. Moreover, the restricted number of published counting uncertainties within various archives hampers a more accurate age estimate. As long as no additional information on counting uncertainties within the individual records is available, applying the standard deviation of circa 2.7% (5.6 years; Extended Data Table 2) covers the known systematic uncertainties and represents the most reliable error estimate of the YD onset in western and central Europe.

### Ice-core assessment of LSE candidates

Volcanic eruption chronologies are commonly derived from increased ice acidity, tephra layers and/or anomalously high sulfate (or sulfur) concentrations measured in polar ice cores[63]. Several ice-core records from Greenland and Antarctica have previously been aligned by identifying common volcanic sulfate peaks[64] (Extended Data Fig. 5). Comparisons between tree-ring $^{14}C$ and ice-core $^{10}Be$ data enables the identification of leads and lags between these two timescales considering similar cosmogenic production rates[33,65–67]. On the basis of new high-resolution tree-ring data, the $^{14}C$ timescale has recently been anchored at a precision of ±8 years (2$\sigma$) during the AL/YD transition[18], whereas the accumulated age error is ±140 years for GICC05 at 13,000 $BP_{GICC05}$ (ref. [23]). However, the absolute dating can be further constrained using cosmogenic isotopes. Best fit is commonly produced if GICC05 is shifted towards younger ages by 1 year (−12/+21 years; 2$\sigma$)[33]. Considering these refined uncertainties, the new LSE age now limits the search window for LSE fallout to 13,015–12,975 $BP_{GICC05}$ (Extended Data Fig. 5). This excludes the bipolar sulfur anomaly at 12,870 $BP_{GICC05}$ (ref. [64]), which was tentatively linked to the LSE[7] and two other major bipolar eruption signals (Extended Data Table 3).

Zooming into the 13,015–12,975 $BP_{GICC05}$ period, a high-resolution (1-cm) sulfate record[68] from the NGRIP[69] ice core depicts several candidate eruptions in this time window (Extended Data Fig. 5 and Extended Data Table 3). The youngest of these, referring to a bipolar sulfate deposition[64] in 12,980 $BP_{GICC05}$, would imply an excessive gas content of the pre-eruption magma reservoir that is unlikely for the LSE. Two years earlier, in 12,982 $BP_{GICC05}$, a particle-rich signal also appears to be unlikely as the composition of glass shards does not match LSE phonolite[70]. Other depositions of insoluble particles[70] and volcanic acids[68] during this time window, recognized for some of the other candidate events (Extended Data Fig. 5 and Extended Data Table 3), present testable hypotheses for future ice-core research. A targeted search for cryptotephra offers the strongest chance of identifying the LSE signature in glacial archives.

### Calibration of $^{14}$C data from Kråkenes Lake

Kråkenes Lake in western Norway[27,36] represents an important independent lacustrine archive of past environmental change and is independently dated using a total of 118 accelerator mass spectrometry $^{14}$C dates performed covering the period from the AL to the Early Holocene. This dataset enables the independent determination of $^{14}$C ages for the important events around the YD cold spell, that is, the AL/YD and the YD–Holocene transitions, as well as interstratified YD Vedde and Early Holocene Saksunarvatn ash layers. Radiocarbon calibration of Kråkenes Lake $^{14}$C ages using the D_Sequence function in OxCal[56,57] and applying the recently released IntCal20[18] dates the AL/YD transition to 12,840–12,699 cal. BP (12,770 ± 71; 2$\sigma$), indicating a shift of the median age estimate by approximately 54 years to older ages compared to IntCal13[71] (Extended Data Table 4). The revised AL/YD transition age estimate for Kråkenes Lake coincides with the proposed date based on the revised LSE age estimate and the consistent 200–213 varve year-long interval from the LSE tephra to the onset of the YD in annually layered records from western and central Europe. The calibrated dates of Vedde (12,153–11,935 cal. BP; 12,044 ± 109; 2$\sigma$) and Saksunarvatn (10,254–10,074 cal. BP; 10,164 ± 90; 2$\sigma$) ashes to IntCal20[18] remain consistent within errors to the results obtained using the IntCal13[71] calibration curve (Extended Data Table 4), as only minor adjustments of the calibration curve were made over this time interval.

## Data availability

Data that support the findings of this study are available from the NOAA/World Data Service for Paleoclimatology data (https://www.ncdc.noaa.gov/paleo/study/33194). Source data are provided with this paper.


41. Park, C. & Schmincke, H.-U. Multistage damming of the Rhine River by tephra fallout during the 12,900 BP Plinian Laacher See Eruption (Germany). Syn-eruptive Rhine damming I. *J. Volcanol. Geotherm. Res.* **389**, 106688 (2020).
42. Waldmann, G. *Vulkanfossilien im Laacher Bims* (Gregor and Unger, 1996).
43. Frechen, J. Die Tuffe des Laacher Vulkangebietes als quartärgeologische Leitgesteine und Zeitmarken. *Fortschr. Geol. Rheinl. Westfal.* **4**, 363–370 (1959).
44. Schweitzer, H.-J. Entstehung und Flora des Trasses im nördlichen Laachersee-Gebiet. *E&G Quat. Sci. J.* **9**, 28–56 (1958).
45. Street, M. *Analysis of Late Palaeolithic and Mesolithic Faunal Assemblages in the Northern Rhineland, Germany*. PhD thesis, Univ. Birmingham (1993).
46. Street, M. Ein Wald der Allerodzeit bei Miesenheim, Stadt Andernach (Neuwieder Becken). *Archäologisches Korrespondenzblatt* **16**, 13–22 (1986).
47. Baales, M., Bittmann, F. & Kromer, B. Verkohlte Bäume im Trass der Laacher See-Tephra bei Kruft (Neuwieder Becken): ein Beitrag zur Datierung des Laacher See-Ereignisses und zur Vegetation der Allerød-Zeit am Mittelrhein. *Archäologisches Korrespondenzblatt* **28**, 191–204 (1998).
48. Brunnacker, K., Fruth, H.-J., Juvigné, E. & Urban, B. Spätpaläolithische Funde aus Thür, Kreis Mayen-Koblenz. *Archäologisches Korrespondenzblatt Mainz* **12**, 417–427 (1982).
49. Rinn, F. *TSAP: time series analyses presentation*. Reference manual v.3.0 (RinnTech, 1996).
50. Synal, H.-A., Stocker, M. & Suter, M. MICADAS: a new compact radiocarbon AMS system. *Nucl. Instrum. Methods Phys. Res. B* **259**, 7–13 (2007).
51. Wacker, L. et al. MICADAS: routine and high-precision radiocarbon dating. *Radiocarbon* **52**, 252–262 (2010).
52. Wacker, L. et al. Radiocarbon dating to a single year by means of rapid atmospheric $^{14}$C changes. *Radiocarbon* **56**, 573–579 (2014).
53. Němec, M., Wacker, L. & Gäggeler, H. Optimization of the graphitization process at age-1. *Radiocarbon* **52**, 1380–1393 (2010).
54. Sookdeo, A. et al. Quality dating: a well-defined protocol implemented at ETH for high-precision $^{14}$C-dates tested on Late Glacial wood. *Radiocarbon* **62**, 891–899 (2020).
55. Kaiser, K. F. *Beiträge zur Klimageschichte vom späten Hochglazial bis ins frühe Holozän: rekonstruiert mit Jahrringen und Molluskenschalen aus verschiedenen Vereisungsgebieten* (Ziegler, 1993).
56. Bronk Ramsey, C. Deposition models for chronological records. *Quat. Sci. Rev.* **27**, 42–60 (2008).
57. Bronk Ramsey, C. Dealing with outliers and offsets in radiocarbon dating. *Radiocarbon* **51**, 1023–1045 (2009).
58. Bird, M. I. in *Encyclopedia of Quaternary Science* (ed. Elias S.A.) 353–360 (Elsevier, 2013).
59. Holdaway, R. N., Duffy, B. & Kennedy, B. Evidence for magmatic carbon bias in $^{14}$C dating of the Taupo and other major eruptions. *Nat. Commun.* **9**, 4110 (2018).
60. Kromer, B., Spurk, M., Remmele, S., Barbetti, M. & Joniello, V. Segments of atmospheric $^{14}$C change as derived from Late Glacial and Early Holocene floating tree-ring series. *Radiocarbon* **40**, 351–358 (1997).
61. Muschitiello, F. & Wohlfarth, B. Time-transgressive environmental shifts across Northern Europe at the onset of the Younger Dryas. *Quat. Sci. Rev.* **109**, 49–56 (2015).
62. Engels, S. et al. Subdecadal-scale vegetation responses to a previously unknown late-Allerød climate fluctuation and Younger Dryas cooling at Lake Meerfelder Maar (Germany). *J. Quat. Sci.* **31**, 741–752 (2016).
63. Sigl, M. et al. Timing and climate forcing of volcanic eruptions for the past 2,500 years. *Nature* **523**, 543–549 (2015).
64. Svensson, A. et al. Bipolar volcanic synchronization of abrupt climate change in Greenland and Antarctic ice cores during the last glacial period. *Clim. Past* **16**, 1565–1580 (2020).
65. Adolphi, F. & Muscheler, R. Synchronizing the Greenland ice core and radiocarbon timescales over the Holocene – Bayesian wiggle-matching of cosmogenic radionuclide records. *Clim. Past* **12**, 15–30 (2016).
66. Adolphi, F. et al. Radiocarbon calibration uncertainties during the last deglaciation: insights from new floating tree-ring chronologies. *Quat. Sci. Rev.* **170**, 98–108 (2017).
67. Muscheler, R., Adolphi, F. & Knudsen, M. F. Assessing the differences between the IntCal and Greenland ice-core time scales for the last 14,000 years via the common cosmogenic radionuclide variations. *Quat. Sci. Rev.* **106**, 81–87 (2014).
68. Ruth, U., Wagenbach, D., Steffensen, J. P. & Bigler, M. Continuous record of microparticle concentration and size distribution in the central Greenland NGRIP ice core during the last glacial period. *J. Geophys. Res.* **108**, 4098 (2003).
69. Bigler, M. et al. Optimization of high-resolution continuous flow analysis for transient climate signals in ice cores. *Environ. Sci. Technol.* **45**, 4483–4489 (2011).
70. Mortensen, A. K., Bigler, M., Grönvold, K., Steffensen, J. P. & Johnsen, S. J. Volcanic ash layers from the Last Glacial Termination in the NGRIP ice core. *J. Quat. Sci.* **20**, 209–219 (2005).
71. Reimer, P. J. et al. IntCal13 and Marine13 radiocarbon age calibration curves 0–50,000 years cal BP. *Radiocarbon* **55**, 1869–1887 (2013).
72. Buizert, C. et al. Abrupt ice-age shifts in southern westerly winds and Antarctic climate forced from the north. *Nature* **563**, 681–685 (2018).
73. Seierstad, I. K. et al. Consistently dated records from the Greenland GRIP, GISP2 and NGRIP ice cores for the past 104 ka reveal regional millennial-scale $\delta^{18}$O gradients with possible Heinrich event imprint. *Quat. Sci. Rev.* **106**, 29–46 (2014).
74. Sigl, M. et al. The WAIS Divide deep ice core WD2014 chronology – part 2: annual-layer counting (0–31 ka BP). *Clim. Past* **12**, 769–786 (2016).
75. Litt, T., Behre, K.-E., Meyer, K.-D., Stephan, H.-J. & Wansa, S. Stratigraphische Begriffe für das Quartär des norddeutschen Vereisungsgebietes. *Eiszeitalt. Ggw. Quat. Sci. J.* **56**, 7–65 (2007).
76. Riede, F. Past-forwarding ancient calamities. Pathways for making archaeology relevant in disaster risk reduction research. *Humanities* **6**, 79 (2017).
77. Patton, H. et al. Deglaciation of the Eurasian ice sheet complex. *Quat. Sci. Rev.* **169**, 148–172 (2017).
78. Zielinski, G. A., Mayewski, P. A., Meeker, L. D., Whitlow, S. & Twickler, M. S. A. 110,000-yr record of explosive volcanism from the GISP2 (Greenland) ice core. *Quat. Res.* **45**, 109–118 (1996).
79. Severi, M. et al. Synchronisation of the EDML and EDC ice cores for the last 52 kyr by volcanic signature matching. *Clim. Past* **3**, 367–374 (2007).



**Acknowledgements** This study was supported by the WSL-internal project 'LSD' and the Swiss National Science Foundation (SNF Grant 200021L_157187/1). U.B. and J.E. received funding from SustES: Adaptation strategies for sustainable ecosystem services and food security under adverse environmental conditions (CZ.02.1.01/0.0/0.0/16_019/0000797). M.S. received funding from the European Research Council under the European Union's Horizon 2020 research and innovation programme (grant agreement no. 820047). We thank A. Hunold, H. Schaaf and B. Streubel for assistance during fieldwork, the University of Hohenheim and M. Friedrich for initial investigations during a DEKLIM-project; and D. Dahl-Jensen and P. Reimer for their constructive feedback that further improved the quality of the manuscript.


**Author contributions** F.R., U.B., O.J. and L.W. designed the study with input from D.N. Tree-ring width measurements were performed by F.R., G.G. and D.N. Radiocarbon measurements and analyses were performed by G.G. and L.W., with the involvement of F.R. L.W. modelled the $^{14}$C. The paper was written by F.R., together with U.B., O.J., J.E., C.O., M.S. and L.W. Further editorial contributions were made by F.A., P.C., S.E., C.L. and A.S. Wood samples were prepared and provided by O.J., H.P., A.L. and S.R. Ice core data were provided and discussed by M.S. and F.A.

**Competing interests** The authors declare no competing interests.

**Additional information**


**Supplementary information** The online version contains supplementary material available at https://doi.org/10.1038/s41586-021-03608-x.



**Correspondence and requests for materials** should be addressed to F.R.



**Peer review information** *Nature* thanks Paula Reimer and the other, anonymous, reviewer(s) for their contribution to the peer review of this work.

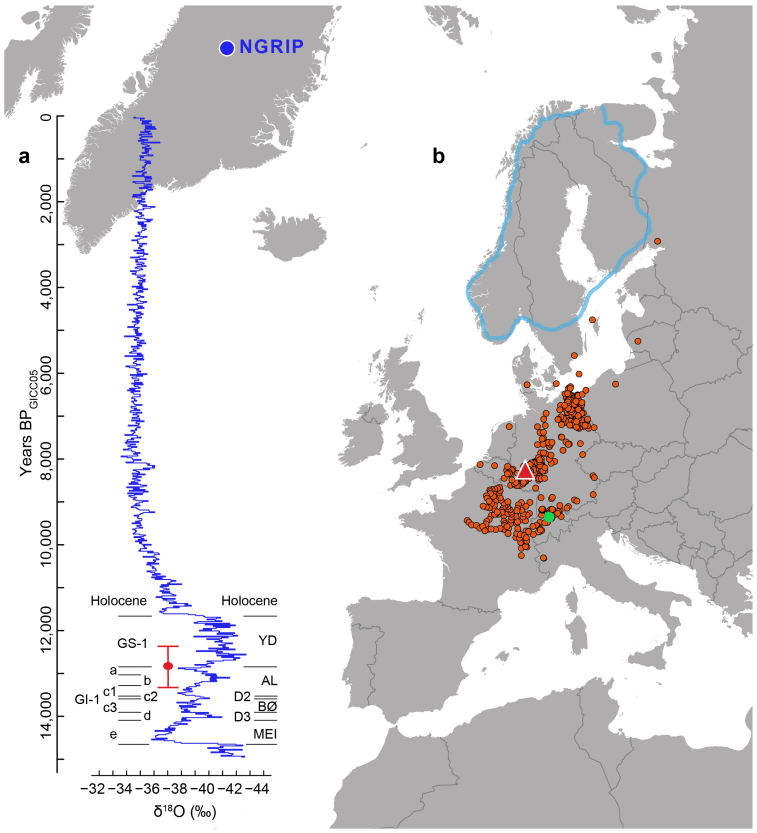


**Extended Data Fig. 1 | Temporal and spatial setting of the Laacher See eruption. a**, Climatic development of the past 15,000 years according to the NGRIP Greenland $\delta^{18}O$ ice core record[23] (blue), covering the Late Glacial and Holocene periods, shown together with the LST $^{40}Ar/^{39}Ar$ age determination[13] at 12,900 ± 560 BP (mean ± 1$\sigma$; red). INTIMATE event stratigraphy[23] of the Late Glacial is outlined left of the NGRIP record, with the European palaeobotanical subdivision of this period[75] aligned on the right. BØ, Bølling interstadial; MEI, Meiendorf interstadial; YD, YD cold interval. Offsets between both schemes are the topic of intensive and ongoing discussion. **b**, Geospatial distribution of LST fallout deposits (orange dots; modified from a previously published study[76]) with locations of Laacher See (red triangle) and the source of the tree stems used to build the Swiss Late Glacial tree-ring and $^{14}C$ records[18] (green dot; SWILM-$^{14}C$). The light blue line indicates the extent of the late AL Fenno-Scandinavian ice sheet (modified from a previously published study[77]). The map was produced using QGIS.

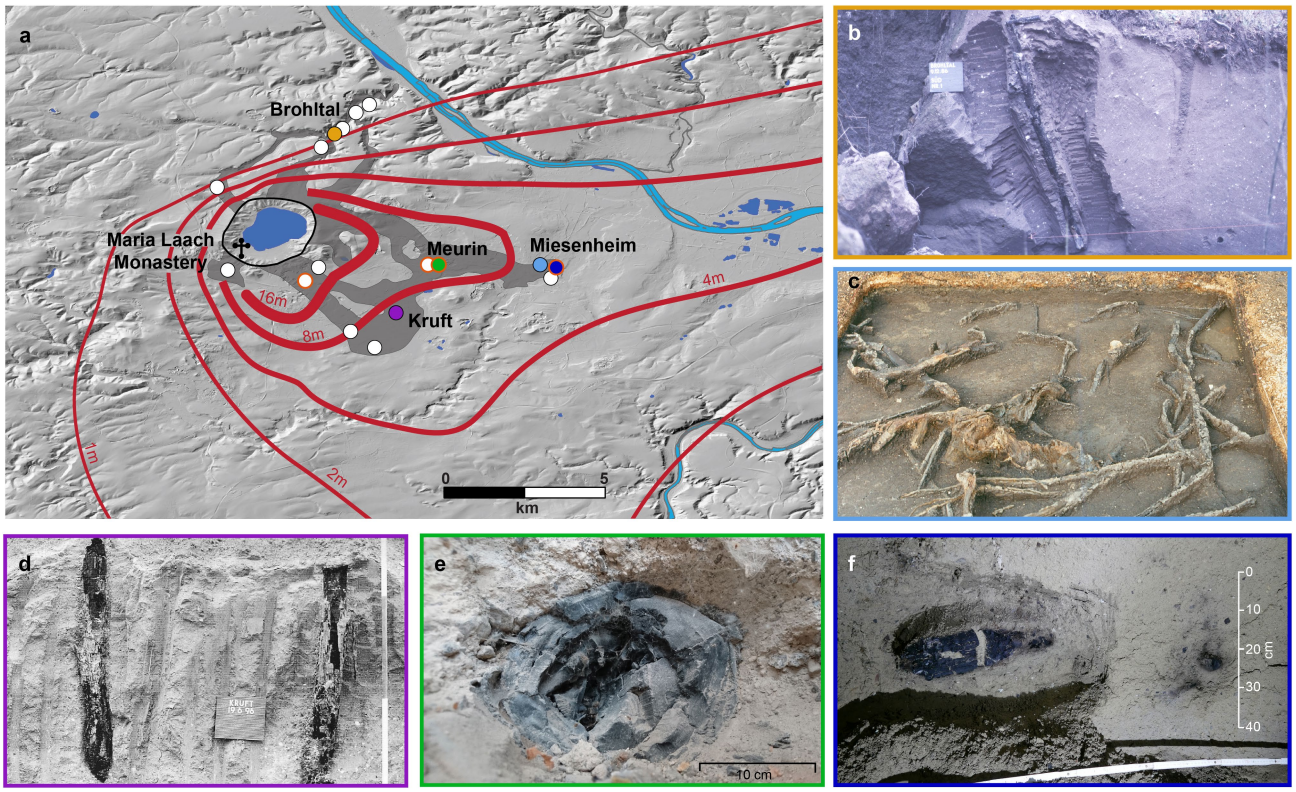


**Extended Data Fig. 2 | Examples of LSE wood finds. a**, Locations of archived (circles with black borders) and newly excavated (in 2019, circles with orange borders) subfossil wood samples within the MLST deposits in the Neuwied Basin (modified from a previously published study[12]). Isopachs for LST fallout are shown in red, and grey shading indicates the extent of MLST ignimbrite deposits. **b**–**f** Subfossil trees from the Brohltal (1986, photograph by E. Turner) (**b**), from an excavated forest at Miesenheim (1986, photograph by M. Street)[46] (**c**), from Kruft (1996, photograph by M. Baales)[47] (**d**); from Meurin (**e**) and an excavation at a new locality in Miesenheim (**f**). Note that only the samples from Brohltahl and Meurin are included in this study, as other materials were exhausted during previous analyses or unsuitable for the performed measurements (see Methods). The map was produced using QGIS. All photographs are provided by the MONREPOS picture archive.

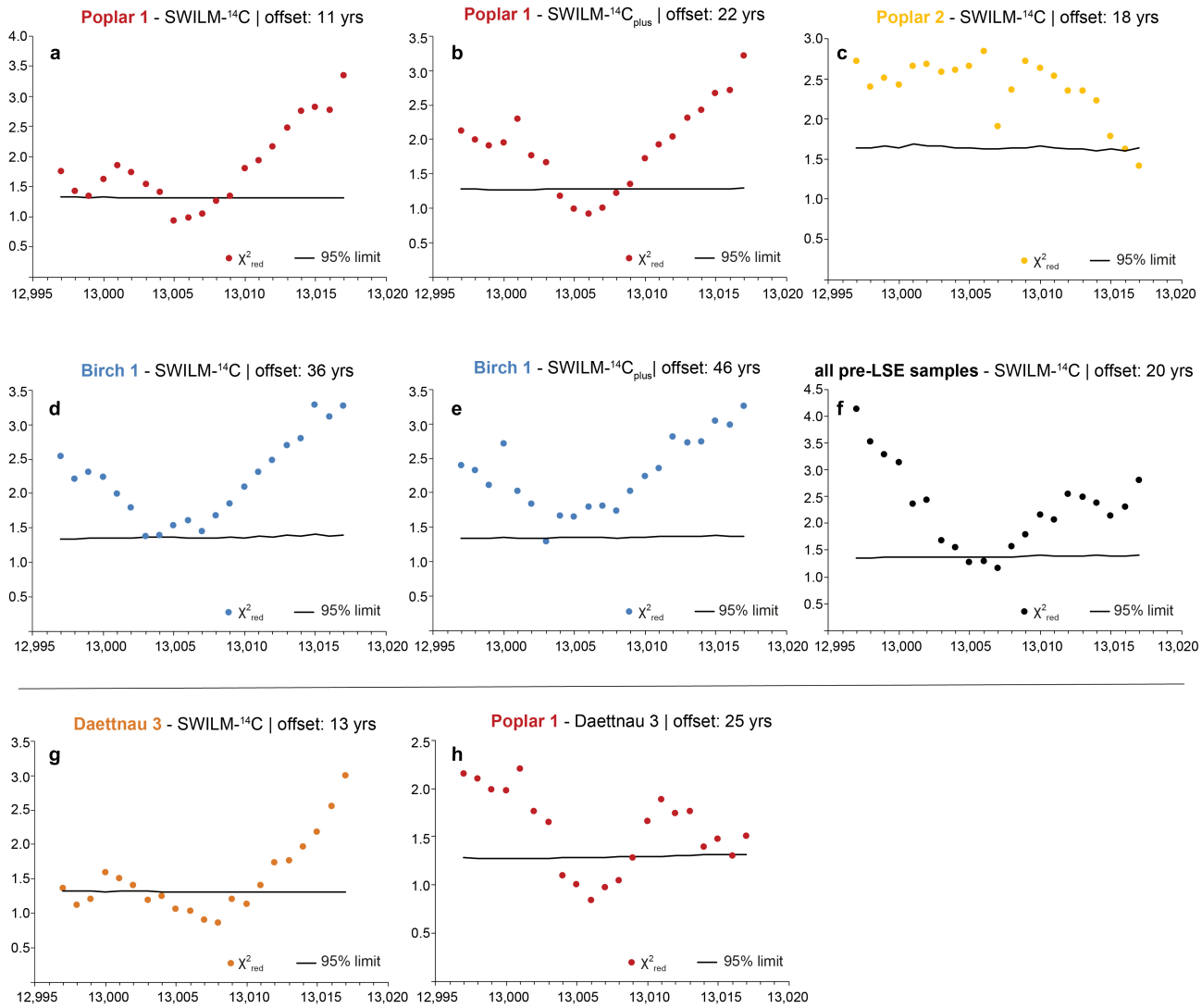


**Extended Data Fig. 3 | Reduced $\chi^2$ test results. a–h**, Most likely $^{14}C$ calendar placement[52] of the last ring of Poplar 1 matched to SWILM-$^{14}C$ with an offset of 11 cal. years (yrs) (**a**); Poplar 1 matched to SWILM-$^{14}C_{plus}$ with an offset of 22 cal. years (**b**); Poplar 2 matched to SWILM-$^{14}C$ with an offset of 18 cal. years (**c**); Birch 1 matched to SWILM-$^{14}C$ with an offset of 36 cal. years (**d**); Birch 1 matched to SWILM-$^{14}C_{plus}$ with an offset of 46 cal. years (**e**); all pre-LSE samples matched to SWILM-$^{14}C$ with an offset of 20 cal. years (**f**); Daettnau 3 matched to SWILM-$^{14}C$ with an offset of 13 cal. years (**g**); and Poplar 1 matched to Daettnau 3 with an offset of 25 cal. years (**h**). Black lines denote to the 95% confidence interval.

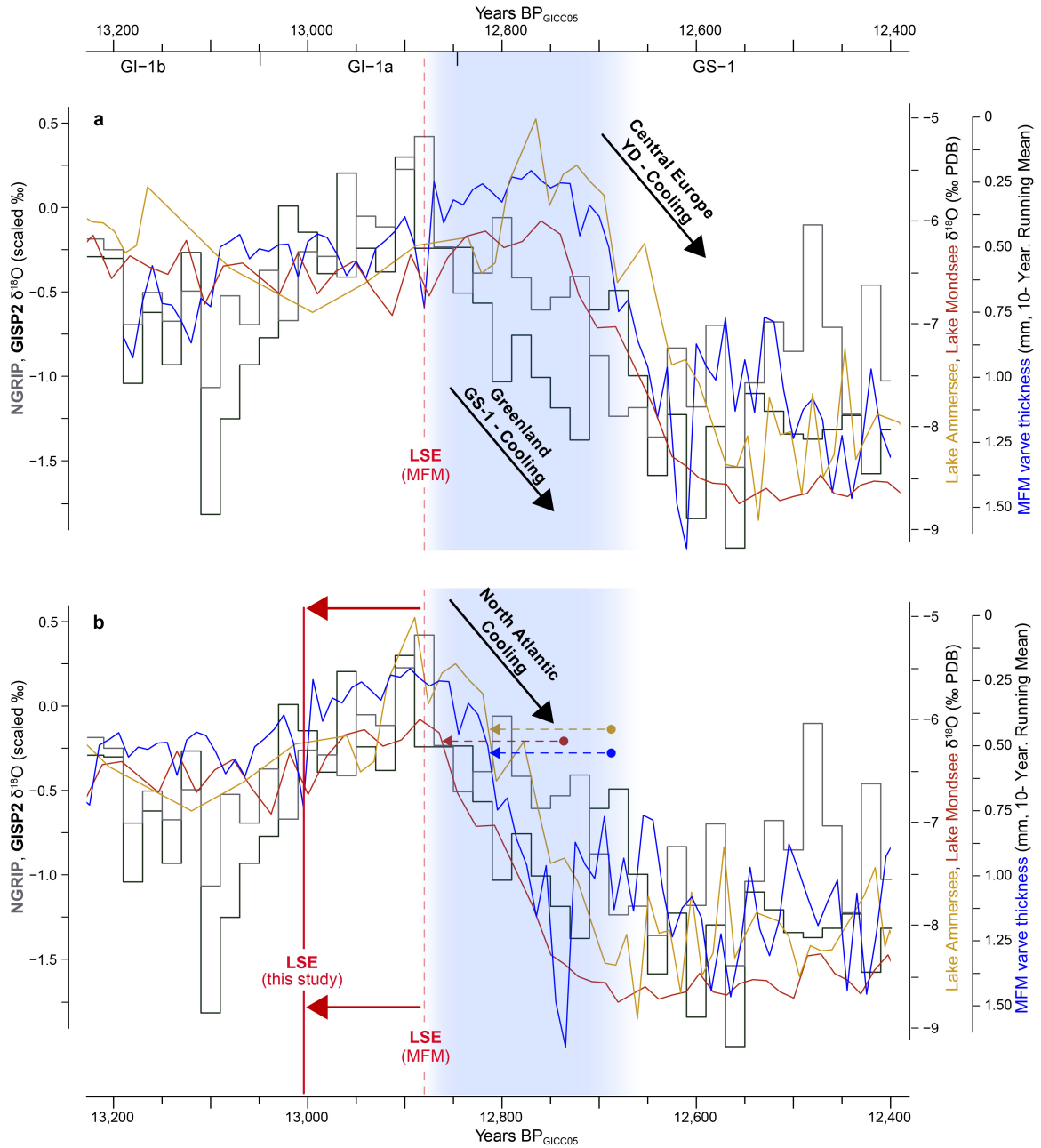


**Extended Data Fig. 4 | Multi-proxy alignment of North Atlantic and European records. a**, NGRIP (grey) and Greenland Ice Sheet Project Two (GISP2) (black) oxygen isotopes ($\delta^{18}O$) at 20-year resolution from Greenland on the GICC05 timescale[23], Alpine $\delta^{18}O$ records from Lake Ammersee[34] (yellow) and Lake Mondsee[35] (red), and MFM[5] (blue) varve thickness plotted as 10-year running means, dated to the MFM timescale with a LSE date of 12,880 $BP_{MFM}$ (±40 years; red dotted vertical line) indicating time-transgressive GS-1 and the YD cooling between 13,200 and 12,400 $BP_{GICC05}$. **b**, The same European proxy records shifted 126 years according to the new LSE date of 13,006 cal.BP (red vertical line)[28] now outlining a synchronized cooling into the GS-1 and YD across the North Atlantic. Blue shading denotes the period of strongest cooling evident in the Greenland ice core isotope records.

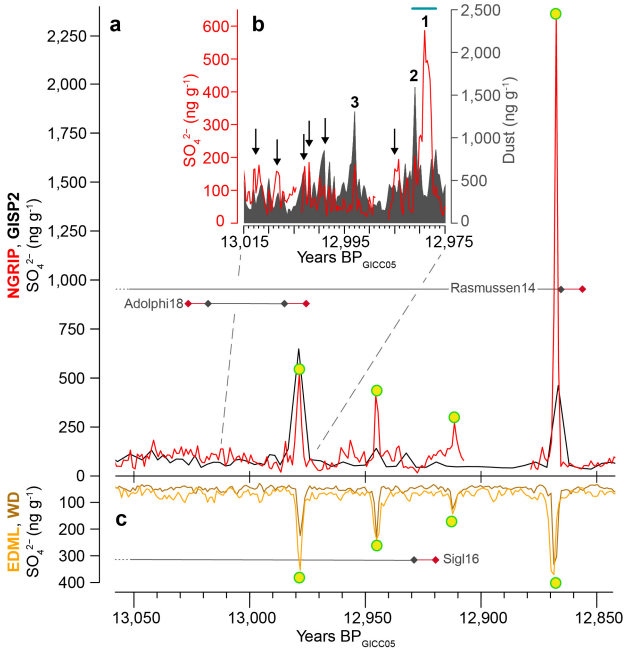


**Extended Data Fig. 5 | Non-sea-salt sulfate and particle records from polar ice cores around the time of the LSE. a**, Ice-core records of sulfate from the Greenland Ice Sheet Project Two (GISP2)[78] and NGRIP[69] records. **b**, High-resolution (1 cm depth) record of sulfate and dust[68] from the NGRIP ice-core record[69] between 13,015 and 12,975 $BP_{GICC05}$ with three volcanic anomalies at 12,980 $BP_{GICC05}$ (1), 12,982 $BP_{GICC05}$ (2) and 12,994 $BP_{GICC05}$ (3; see Extended Data Table 3). Black arrows indicate additional obtained sulfate peaks; the cyan bar denotes the 17-cm sampling range in which tephra shards were previously detected and characterized[70] encompassing two distinct volcanic signals (1 and 2). **c**, Ice-core records of sulfate (calculated from sulfur measurements) from West Antarctic Ice Sheet Divide (WD)[74] and Dronning Maud Land (EDML)[79] ice core. All ice cores are synchronized[65,72,73] on the GICC05 chronology[23] timescale with respect to AD 1950. Grey horizontal lines represent the accumulated age error in 13,000 BP with ±105 years for WD2014[74] and ±140 years for GICC05[23], which has been further reduced (−12/+21 years; 2$\sigma$) based on the synchronization of tree-ring $^{14}C$ and ice-core $^{10}Be$[33]. Red horizontal lines outline the added LSE $^{14}C$ uncertainty (±9 years). Yellow dots denote the obtained bipolar sulfate anomalies.

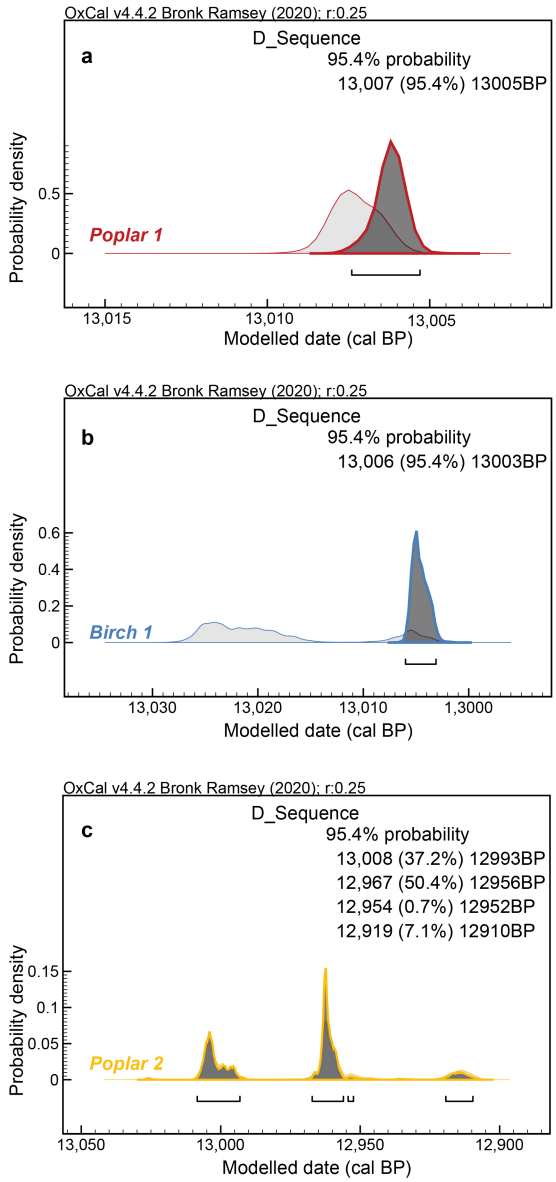


**Extended Data Fig. 6 | D_Sequence wiggle-matching results with OxCal.** **a**–**c**, All radiocarbon ($^{14}C$) modelled LSE ages obtained from Poplar 1 (**a**), Birch 1 (**b**) and Poplar 2 (**c**), applying the extended Swiss Late Glacial Reference (SWILM-$^{14}C_{plus}$) point to a similar eruption date. Whereas the long-lived Poplar 1 and Birch 1 exceed the $^{14}C$ plateau with the initial $^{14}C$ dates, Poplar 2 provide three possible wiggle-match placements; however, under the constraint that this sample was also found within the MLST deposits, the two younger $^{14}C$ results need to be excluded.

## Extended Data Table 1 | Pre-LSE chronology

| Sample | Nr. of tree rings | Nr. of $^{14}C$ dates | $^{14}C$ date/ tree-ring ratio | Outer most complete ring (Yes/ Now) | Bark (Yes/ Now) | Start date prior to LSE | End date prior to LSE |
|---|---|---|---|---|---|---|---|
| *Poplar 1* | 95 | 85 | 0.90 | Y | Y | 95 | 0 |
| *Poplar 2* | 54 | 16 | 0.30 | N | N | 57 | 3 |
| *Birch 1* | 104 | 50 | 0.48 | Y | N | 105 | 1 |
| *Birch 2* | 63 | - | - | Y | N | 64 | 1 |
| *Birch 3* | 72 | - | - | Y | Y | 72 | 0 |

Dendrochronological characteristics and performed radiocarbon ($^{14}C$) measurements.

## Extended Data Table 2 | Annually varved layer estimate of the YD onset relative to the LST

| Record | Country | LST to YD onset (avl) | Counting error (± avl) |
|---|---|---|---|
| Meerfelder Maar[5] | Germany | 200 | 2 |
| Rehwiese[29] | Germany | 205 | 3 |
| Soppensee[39] | Switzerland | 213 | Not published |
| Trzechowskie[40] | Poland | 203 | 3 |
| Mean | | 206 | 5.6 |

Data include published information on the counting uncertainty for all available annually laminated records[5,29,39,40] in western and central Europe. The mean is derived from the average of all records and their standard deviation.

## Extended Data Table 3 | Volcanic sulfate depositions in Greenland and Antarctica around the new LSE date

| Age GICC05 | ID | Signal within LSE search window | Enrichment in insoluble particles | Bipolar sulphate signal[65] | Depth NGRIP | Annual peak sulphate NGRIP | Depth WD | Annual peak sulphate WD |
|---|---|---|---|---|---|---|---|---|
| Yrs BP (1950) | | | | | m | ng $g^{-1}$ | m | ng $g^{-1}$ |
| 12,870 | | no | N/A | yes | 1527.40 | 2279 | 2083.17 | 333 |
| 12,913 | | no | N/A | yes | 1529.04 | 259 | 2086.68 | 126 |
| 12,946 | | no | N/A | yes | 1530.52 | 392 | 2089.70 | 234 |
| 12,980 | 1 | yes | yes | yes | 1531.86 | 504 | 2092.86 | 225 |
| 12,982 | 2 | yes | yes | no | 1531.91 | 165 | N/A | N/A |
| 12,985 | | yes | no | no | 1532.08 | 168 | N/A | N/A |
| 12,994 | 3 | yes | yes | no | 1532.43 | 92 | N/A | N/A |
| 13,000 | | yes | yes | no | 1532.68 | 100 | N/A | N/A |
| 13,013 | | yes | no | no | 1533.20 | 130 | N/A | N/A |
| Median sulphate concentration (13,015-12,975 yrs $BP_{GICC05}$) | | | | | | 71 | | 48 |

Ice-core ages refer to the GICC05 chronology[23] with respect to AD 1950 and are derived from previous volcanic synchronizations[65,72,73]. Volcanic sulfate deposition data for Greenland[68] and Antarctica[74] were published previously. NA, not available.

**Extended Data Table 4 | OxCal calibration results of $^{14}$C-dated events from the Kråkenes core chronologies**

| Boundary/Event | IntCal13 | | | IntCal20 | | |
|---|---|---|---|---|---|---|
| | 95.4% CI | Mean ± 1σ | Median | 95.4% CI | Mean ± 1σ | Median |
| Saksunarvatn Ash | 10,282 – 10,137 | 10,210 ± 35 | 10,210 | 10,257 – 10,074 | 10,178 ± 45 | 10,185 |
| YD/Holocene | 11,674 – 11,431 | 11,546 ± 59 | 11,542 | 11,636 – 11,409 | 11,519 ± 56 | 11,521 |
| Vedde Ash | 12,151 – 11,981 | 12,066 ± 42 | 12,067 | 12,149 – 11,934 | 12,043 ± 53 | 12,043 |
| AL/YD | 12,825 – 12,615 | 12,711 ± 52 | 12,705 | 12,840 – 12,699 | 12,766 ± 36 | 12,759 |

Confidence interval (CI), mean and median values are given in cal. BP (AD 1950). Kråkenes core chronologies[27,36] were analysed using IntCal13[71] and IntCal20[18].